



HAL
open science

Cyan $\text{Ni}_{1-x}\text{Al}_{2+2x/3} \text{x}/3\text{O}_4$ single phase pigments synthesis and modification for electrophoretic inks formulation

Béatrice Serment, Manuel Gaudon, Alain Demourgues, Amélie Noël, Guillaume Fleury, Eric Cloutet, Georges Hadziioannou, Cyril Brochon

► To cite this version:

Béatrice Serment, Manuel Gaudon, Alain Demourgues, Amélie Noël, Guillaume Fleury, et al.. Cyan $\text{Ni}_{1-x}\text{Al}_{2+2x/3} \text{x}/3\text{O}_4$ single phase pigments synthesis and modification for electrophoretic inks formulation. ACS Omega, 2020, 10.1021/acsomega.0c01289 . hal-02908162

HAL Id: hal-02908162

<https://hal.science/hal-02908162v1>

Submitted on 28 Jul 2020

HAL is a multi-disciplinary open access archive for the deposit and dissemination of scientific research documents, whether they are published or not. The documents may come from teaching and research institutions in France or abroad, or from public or private research centers.

L'archive ouverte pluridisciplinaire **HAL**, est destinée au dépôt et à la diffusion de documents scientifiques de niveau recherche, publiés ou non, émanant des établissements d'enseignement et de recherche français ou étrangers, des laboratoires publics ou privés.

Cyan $\text{Ni}_{1-x}\text{Al}_{2+2x/3}\text{O}_4$ single phase pigments synthesis and modification for electrophoretic inks formulation.

Béatrice Serment^{†‡}, Manuel Gaudon,^{†} Alain Demourgues[†], Amélie Noël[‡], Guillaume Fleury[‡],
Eric Cloutet[‡], Georges Hadziioannou[‡] and Cyril Brochon,^{‡*}*

[†] CNRS, Univ. Bordeaux, Bordeaux INP, ICMCB, UMR 5026, F-33600 Pessac, France

[‡] CNRS, Univ. Bordeaux, Bordeaux INP, LCPO, UMR 5629, F-33615, Pessac, France

KEYWORDS

Electrophoretic inks, cyan pigment, spinel, hybrids particles, Pechini, dispersion polymerization

ABSTRACT

Cyan $\text{Ni}_{1-x}\text{Al}_{2+2x/3}\text{O}_4$ single phase pigments with various Ni:Al atomic ratios (from 1:2 down to 1:4) have been prepared by sol gel route (Pechini) followed by post-annealing treatments. Nickel aluminates crystallize in the well-known spinel structure (Fd-3m space group) where metals are located at two different Wyckoff positions: *16d* (octahedron) and *8a* (tetrahedron). Based on XRD Rietveld refinements, Ni^{2+} cations are shown to be partially located in both tetrahedral and octahedral sites and, in addition, cationic vacancies occupy Oh environment. In the pure phase series, Ni/Al = 0.35, 0.40, 0.45, as the Al content increases, the Ni^{2+} rate in Td site decreases for Ni/Al=0.45, thus altering the cyan color ; within this series, the most saturated cyan coloration is reached for the highest Al concentration. Inorganic pigment drawbacks are their high density and hydrophilic surface, which induced sedimentation and aggregation in non-polar media used in electrophoretic inks. Hybrid core shell particles pigments have been synthesized from cyan pigments by using nitroxide mediated radical polymerization (NMRP) with methyl methacrylate monomer in isopar G leading to a dispersion of electrically charged hybrids in apolar media. Surface functionalization of the pigments by OTS and DTS modifiers have been compared. The

inorganic pigments are successfully encapsulated by organic shells to allow a strong decrease of their density. Cyan inks, adequate for their use in e-book readers or other electrophoretic displays, taking further advantage of the high contrast ratio and reflectivity of inorganic pigments as regards to organic dyes, have been stabilized.

1. INTRODUCTION

Electrophoretic image displays (EPID) raise a strong interest since the first studies of Jacobson *et al.*^{1,2} describing the high potential of these new displays: low cost, ultralow power consumption, good flexibility and reliability. The commercialized black/white electronic books such as Kindle by Amazon[®] are still the most developed applications for EPID in the market despite of potential broader applications.³ Actually, most of e-books readers are in grey scale even if 3-colours systems thanks to the use of colour-filters have been recently emerging^{4,5}. This type of colour system is not as effective as the use of pigments. Moreover, few studies reported the synthesis of coloured electrophoretic inks with the encapsulation of dyes to obtain chromatic EPID^{4,6-8}. The required properties to obtain performant EPID are mainly high surface charges, a good dispersion stability of the pigment particles and low inter-particles interactions to ensure the long-term electrophoretic control of the ink coloration⁹. Electrophoretic inks are typically prepared in a low-cost electrophoretic medium such as Isopar G. The use of inorganic pigments allows a high contrast ratio and reflectivity of the ink with no loss of coloration with time compared with encapsulated dyes. Actually, Wen *et al.* have demonstrated that polymer particles filled with a dye have a reflectance spectrum that decrease over 30% after 56h¹⁰. Due to this bottleneck, it is preferable to use inorganic pigment to reach good contrast and long-term stability. Nevertheless, inorganic pigments suffer from their high density and hydrophilic surface, which induce sedimentation and aggregation in non-polar media. To tackle these challenges, the inorganic pigments must be encapsulated in an organic shell allowing a decrease of both the strength of the interactions between the particles and the overall density¹¹.

Cyan pigments are obviously of a great interest, because cyan is one of the three subtractive colours. Cyan pigments from copper and nickel phthalocyanines have been used as hybrid particles for photoelectrophoretic imaging processes¹². Copper is an adequate chromophore cation for cyan pigment application: copper being associated with cyan coloration into inorganic oxides since, for instance, copper is the chromophore cation in the turquoise natural stone (Cu-doped $\text{CaAl}_6(\text{PO}_4)_4(\text{OH})_8 \cdot 4\text{H}_2\text{O}$ chemical composition). Beautiful cyan hues were recently synthesized using copper-based phosphates even if a very low saturation hinders further applications (pale

pigments with too high luminosity)¹³. In our own research group, cyan pigments have been already developed using nickel chromophore in spinel structure implying a distribution of nickel ion in octahedral and tetrahedral sites: $Zn_{1-x}Ni_xAl_2O_4$ solid solutions showed a colour shift from green to blue, due to the modulation of the cationic distribution in the aluminate spinel lattice¹⁴. Spinel-type oxide represents one of the most studied class of materials in the solid-state science because of their relevant magnetic, refractory, semi-conducting and colouring properties. The incorporation of transition metal ions into stable diamagnetic spinels is a successful methodology to obtain materials with a very intense colour. This structure features the general AB_2O_4 formula in which A and B are cations occupying tetrahedral and octahedral sites. Assuming A^{2+} and B^{3+} cations, there are two ideal crystallographic structures: the first one is the direct spinel, in which the tetrahedral sites are occupied by A^{2+} cation and the octahedral sites by the B^{3+} cation; the second one is the inverse spinel, in which all tetrahedral sites are occupied by B^{3+} cation, while A^{2+} and B^{3+} cations share in equivalent proportion the octahedral sites^{15, 16}. In the $NiAl_2O_4$ structure, the cation arrangement is typical of a partially inverse spinel $(Ni_{1-z}Al_z)[Ni_zAl_{2-z}]O_4$, in which Ni^{2+} and Al^{3+} are randomly located in both tetrahedral and octahedral positions respectively. $NiAl_2O_4$ pigments have been prepared by various routes such as sol-gel^{17, 18}, solid state reaction¹⁹, microwave^{20, 21}, sonochemical²², Pechini method²³, thermal decomposition of polynuclear malate complex²⁴, mechano-chemical synthesis²⁵, and combustion route^{26, 27}.

However, it is still difficult to prepare the stoichiometric $NiAl_2O_4$ because of the persistent NiO impurity even if the Ni:Al 1:2 molar ratio is well controlled. For instance, Cooley and Reed²⁸ have shown the occurrence of NiO impurity in the final compound despite heat treatments performed at 1664 K for 2 days. In the same way, Han *et al.* have studied the effect of the sintering temperature and time for this bi-phasic system and showed that there is no mean to reduce the NiO impurity quantity starting from a Ni:Al 1:2 stoichiometric mixture even after very long treatment at high temperatures²⁹. This residue of NiO besides the $NiAl_2O_4$ main compound, which is of dark green coloured, drastically limits the application of nickel aluminate spinel as cyan pigment. To overtake this problem, Subramanian *et al.*³⁰ prepared over-stoichiometric aluminum compounds leading to a pure-phase sample with a $Ni_{0.91}Al_{2.06}O_4$ composition.

This paper firstly deals with the elaboration of $Ni_{1-x}Al_{2+2x/3}O_4$ (the Ni/Al atomic ratio varying from 1:2 to 1:4) using the sol-gel synthesis known as Pechini route. The as-prepared gels were subsequently submitted to post-annealing treatments under air. The resulting powders were characterized by XRD Rietveld refinements combined with diffuse reflectance and TEM analysis. In a second part, these powders have been firstly modified by silanes chains and these hybrid

particles were then formulated by a nitroxide mediated radical polymerization of MMA (NMRP) in Isopar G. The inks have been characterized by turbidity measurements to evaluate their stability over time. Charge, electrophoretic mobility, density and particles diameter have been also measured and these parameters were correlated with the ink stability.

2. RESULTS AND DISCUSSION

Synthesis and characterization of the $NiAl_{2+x}O_{4+\square}$ compounds

The $Ni_{1-x}Al_{2+2x/3}O_4$ pigments with different Ni/Al molar ratios (from 0.25 up to 0.5 (Ni/Al = $1-x/(2+2x/3) = 0.25; 0.30; 0.35; 0.40; 0.45$ and 0.5 ; *i.e.* 6 $Ni_{1-x}Al_{2+2x/3}O_4$ samples from $x \sim 0.4$ down to $x = 0$) were prepared using the Pechini sol-gel route followed by a post-annealing under air atmosphere at 1400°C to ensure the cationic homogenization.

The X-ray diffraction patterns of the as-prepared powders are reported in **Figure 1**. On the basis of XRD data, a single spinel phase is obtained for Ni/Al molar ratios between 0.35 and 0.45. For the extreme Ni/Al ratios (0.25, 0.30 and 0.5), biphasic systems are observed. Indeed, a NiO phase (with R-3m space group and where Ni^{2+} are located in octahedral sites) is detected for the 0.50 Ni/Al ratio while a $\alpha\text{-Al}_2\text{O}_3$ alumina phase (with R-3c space group and where Al^{3+} are located in octahedral sites) is retrieved for the 0.30 and the 0.25 Ni/Al ratios. To estimate the proportion of each phase, to refine unit-cell parameters of the main spinel phase and also, to get an idea of the $Ni^{2+}\text{-}Al^{3+}$ cationic distribution inside the spinel framework, Rietveld refinements of XRD patterns were performed. First, as shown in the **Figure 2**, a decrease of the spinel unit-cell parameter, from 8.048 \AA up to 8.005 \AA , is noticed with the increase of Al content for monophasic powder. This tendency is particularly apparent for samples with Ni/Al atomic ratio varying between 0.35 and 0.45. Such an evolution is related to the evolution of the ionic radii for Ni^{2+} and Al^{3+} depending on their localization (0.55 \AA and 0.39 \AA in tetrahedral site for Ni^{2+} and Al^{3+} , respectively and 0.69 \AA and 0.535 \AA in octahedral site for Ni^{2+} and Al^{3+} , respectively). However, as Al content increases, the stabilization of cationic vacancies should contribute to a decrease of the reticular energy and the coulombic interactions, and could thus be associated to an increase of the cell parameter. To strengthen the discussion, one can argue that the $\alpha\text{-Al}_2\text{O}_3$ oxide with spinel structure (and a chemical formulae which can be written as $Al_{8/3}\square_{1/3}O_4$), exhibits a cell parameter close to that of $NiAl_2O_4$ spinel ($7.90 \text{ \AA} < a < 7.95 \text{ \AA}$, ^{31, 32}), despite the occurrence of only Al^{3+} , but thanks to its high vacancy rate. Thus, the decrease of unit-cell parameter with Al content is not as large as expected because of the compensation from the cationic vacancies.

Each phase proportion has been obtained from Rietveld refinement of all the phases indexed on the XRD diagrams and is also reported in the **Figure 2**. For a Ni/Al=0.50 ratio, there is 96 % of spinel phase and 4% of NiO. For Ni/Al ratios equal to 0.25 and 0.30, there is respectively 72% and 98% of NiAl₂O₄ and 28% and 2% of Al₂O₃ phases. Further investigation was performed on the Ni/Al = 0.4 pure sample in order to extract the cationic distribution (between Al³⁺, Ni²⁺ and vacancies) in the tetrahedral site-octahedral site cationic sub-network. The Ni/Al = 0.4 sample gets a chemical composition which can be written as Ni_{0.84}Al_{2.11}□_{0.05}O₄. Unfortunately, the occupancies of the tetrahedral and octahedral sites are impacted by the Ni-Al inversion rate as well, in the same time, as the positioning of the vacancies. Hence, a choice has to be made in the refinement process and we proposed to perform and compare three refinements procedure: (i) a first refinement considering NiAl₂O₄ stoichiometric composition, for which the occupancies between tetrahedral and octahedral site is impacted only by the Ni-Al inversion rate: *i.e.*, only the *z* inversion parameter assuming the (Ni_{1-z}Al_z)[Ni_zAl_{2-z}]O₄ crystal framework is refined; (ii) a second refinement considering all cationic vacancies are located into octahedral sites, *i.e.*, assuming (Ni_{0.84-z}Al_{0.16+z}) [Al_{1.95-z}Ni_z□_{0.05}]O₄ composition; (iii) a third refinement considering all cationic vacancies are located into tetrahedral sites, *i.e.*, assuming (Ni_{0.84-z}Al_{0.11+z}□_{0.05}) [Al_{2.00-z}Ni_z]O₄ composition.

In the **Figure SI-1**, considering the experimental XRD diffractogram of the Ni/Al = 0.4 sample, the three difference signals between calculated and experimental data obtained from the three refinement procedures, are superimposed. No significant difference between the qualities of the refinements (taking into account the R_B reliability factor on **Table 1**) is observed comparing the different applied processes, even if the location of the vacancies into octahedral sites (*i.e.* model II) tends to show that this is the best option. This is confirmed by the correlation factors issued from the three refinement procedures, which are reported in the **Table 1**. Hence, it is very difficult to conclude on the exact cation distribution inside the spinel network. Interestingly, one can note that the calculated quantity of nickel and aluminum located in octahedral or tetrahedral sites are strongly influenced by the refinement process. As illustration, the ratios between the nickel in tetrahedral site and the nickel in octahedral site equals 0.18/0.82=0.22, 0.39/0.45=0.87 and 0.55/0.29=1.89 for the first, second and third refinement processes, respectively. Thus, the chromophore ion (nickel ion) distribution into the tetrahedral and octahedral sites, which governs the colorimetric properties of the spinel compounds, is difficult to precisely assert. This last point will be discussed in the following section as regards to UV-Visible and optical absorption properties around Ni²⁺ chromophores stabilized in Oh and Td sites.

TEM investigations combined with EDS analyses of $\text{Ni}_{1-x}\text{Al}_{2+2x/3}\text{O}_4$ pigments with a (Ni/Al) ratios equal to 0.25 and 0.40 were performed. The aim is to analyze and compare the morphology of the biphasic or monophasic samples (particle sizes of the spinel, NiO and Al_2O_3 phases) and to check the cation distribution (Ni^{2+} and Al^{3+} cation distribution). **Figure 3** shows the TEM images collected on the three analyzed samples and the atomic percentage of each cation in various areas is indicated on TEM images. The first micrograph (**Figure 3**, left side) corresponding to the Ni/Al = 0.4 sample, confirms the occurrence of a monophasic sample, since it exhibits some crystallites with isotropic morphology (with roughly 20-30 nm diameter) partially aggregated. The unique Ni/Al local ratio, *i.e.* a homogeneous cationic distribution observed in the whole sample, is calculated to 0.41 (average value), a value in perfect agreement with the target composition. However, one can observe a multimodal and large particle size distribution for the two biphasic samples with a Ni/Al ratio equal to 0.40 or 0.25 respectively. For illustration, for the sample Ni/Al = 0.25, a bimodal particle size distribution is clearly evidenced with a first sub-population of particles with a diameter about 10 nm and a second sub-population with particles size about 30 nm (central image, **Figure 3**). Significant deviations of the Ni/Al ratio are shown depending on the analyzed area. Furthermore, large and isolated aggregates constituted of faceted crystals are also observed on this sample (right panel, **Figure 3**). The STEM analyses show that the big aggregates are very rich in aluminum cation and should correspond to the corindon-type phase detected in the X-ray diffraction patterns. This Ni/Al = 0.25 sample, in agreement with the XRD analyses, exhibits the occurrence of two phase-types: one spinel-type phase with a non-homogeneous Ni/Al ratio and one corundum-type ($\alpha\text{-Al}_2\text{O}_3$) phase.

UV-Vis-NIR absorbance curves (Kubelka Munk transforms) are superimposed for the various as-prepared samples in **Figure 4**. In perfect agreement with X-ray diffraction pattern refinement showing that the $\text{Ni}_{1-x}\text{Al}_{2+2x/3}\text{O}_4$ compounds are partially inverse, the d-d transitions associated to the nickel chromophore in tetrahedral (red transitions) and octahedral (blue transitions) coordination are apparent on the optical spectra in all cases. Five bands are observed, two of them are centered at 400 nm and 700 nm and can be attributed to the nickel (II) ion in octahedral coordination with ${}^3\text{A}_{2g}(\text{F}) \rightarrow {}^3\text{T}_{1g}(\text{P})$ and ${}^3\text{A}_{2g}(\text{F}) \rightarrow {}^3\text{T}_{1g}(\text{F})$ transitions, respectively. A first high energy triplet indexed as a ${}^3\text{T}_1(\text{F}) \rightarrow {}^3\text{T}_1(\text{P})$ transition (due to the L-S Russel-Saunders coupling) is observed in the visible range at 650 nm, while a second low energy triplet in the NIR range (between 1500 and 3000 nm) can be indexed as a ${}^3\text{T}_1(\text{F}) \rightarrow {}^3\text{T}_2(\text{F})$ transition. Both triplets can be associated with nickel(II) ion in a tetrahedral coordination. The last large multiplet centered at 1150 nm is more difficult to index because it could correspond to the superimposition of transitions

taking their origin for nickel (II) ion in both [4] and [6] coordination numbers: the ${}^3T_1(F) \rightarrow {}^3A_2(F)$ transition for the four-fold coordinated site and the ${}^3A_{2g}(F) \rightarrow {}^3T_{2g}(F)$ transition considering an octahedral environment. The Racah parameter and crystal field splitting of Ni^{2+} ($3d^8$) in each site have been calculated based on Tanabe-Sugano diagrams (d^2 for $Ni^{2+}[Td]$ and d^8 for $Ni^{2+}[Oh]$)³³⁻³⁶. The results are $B_{Ni^{2+}(Td)} = 812 \text{ cm}^{-1}$ ($10Dq = 0.57 \text{ eV}$) and $B_{Ni^{2+}(Oh)} = 860 \text{ cm}^{-1}$ ($10 Dq = 1.06 \text{ eV}$). Moreover, nephelauxetic effect can be calculated with $B_{free} = 1041 \text{ cm}^{-1}$ and $\beta(Ni^{2+}(Td)) = 0.78$ and $\beta(Ni^{2+}(Oh)) = 0.83$, in good agreement with the stronger covalent character of Ni-O bond in Td site. Indeed, the absorption bands for the Ni^{2+} in tetrahedral sites are centered at 2551 nm and at 1150 nm in the near infrared region. About the Ni^{2+} in octahedral site, the second transition corresponds to the absorption band centered at 1162 nm. Furthermore, for all samples, a charge transfer band (CTB) is located at about 350 nm and associated to $O^{2-} \rightarrow Ni^{2+}$ electronic transfer, as expected for this kind of wide-gap semi conducting oxide. Besides an absorption band is observed at 776 nm and can be attributed to the ${}^3T_1(F) \rightarrow {}^1E(D)$ forbidden transition of the Ni^{2+} in tetrahedral site. Moreover, one can see that the band intensity centered at 650 nm evolves significantly versus the Ni/Al molar ratio. Indeed, there is an increase of the K/S absorption when the Ni/Al ratio decreases from 0.5 to 0.4 and a drop of intensity after 0.4.

Two effects affect the compounds coloration: the purity of the as-prepared spinel phase and the intensity of the visible absorption bands, especially the evolution of the more intense visible band (the triplet located at about 650 nm related to Ni^{2+} in tetrahedral site). L^* , a^* and b^* colour parameters were extracted from diffuse reflectance curves, what allows the $L^*a^*b^* \rightarrow RGB$ colour space transformation, the representation of the colour of each compound has been done with any common software (**Figure 4, inset**). All the samples exhibit a cyan coloration with strongly negative a^* hue parameter (green-red axis), *i.e.* an important green component, and strongly negative b^* parameter (blue-yellow axis), *i.e.* an important blue component. For supporting the discussion, one can remind that the most saturated cyan which can be imagined, corresponding to RGB trichromatic parameters with a null red component and the maximal value for both green and blue components, is associated to $L^* = 62.6$; $a^* = -33.7$; $b^* = -41.6$. The as-prepared compounds exhibit beautiful and intense cyan coloration with $L^* = 51.81$; $a^* = -23.11$; $b^* = -30.80$ for the Ni/Al=0.4 composition. When the system is biphasic with NiO impurity, the colour is more greenish (for Ni/Al = 0.5 molar ratio the b^* parameter is less negative) and this can be reasonably attributed to the green colour of the NiO particles. When the system is biphasic with $\alpha\text{-Al}_2\text{O}_3$ impurity, an increase of the L^* luminosity parameter is observed from 51-54 for the pure spinel sample up to 55-57 for the spinel in presence of Al_2O_3 impurity and this can be reasonably

attributed to the white colour of Al₂O₃ pure phase. It is noteworthy that the increase of the green component of the color for the Ni/Al = 0.25 sample with large part of alumina impurity, is probably associated to the insertion of Ni²⁺ ion into these α -alumina phase (exhibiting octahedral coordination sites, only). The three pure spinel samples (Ni/Al = 0.35, 0.40 and 0.45) exhibit very similar L*, a* and b* parameter. However, a careful comparison of evolution of band intensities in this series, associated to Td site (triplet around 650 nm corresponding to ³T₁ (F) → ³T₁ (P) transition) and around 700 nm related to octahedral coordination (³A_{2g}(F) → ³T_{1g} (F) transition) seems to show that the Ni²⁺ occupancy in Td site is maximum for Ni/Al atomic ratio equal to 0.4 and 0.35. The acentric character of Td site leads to high intensity of associated bands compared to those related to Oh site where the local environment is centrosymmetric. Indeed, for Ni/Al = 0.45 composition, the triplet intensity around 650 nm associated to Td site decreases more compared to that of other atomic ratio, whereas the band intensity related to Oh environment remains maximum and comparable to the Ni/Al=0.40 composition. It means in first approximation that the Ni²⁺ rate in Oh coordination raises as the Al content decreases and the composition with the best cyan hue can be optimized as the Ni²⁺ rate in Td site is maximum. Thereafter, the Ni/Al molar ratio equal to 0.40: Ni_{0.84}Al_{2.11}O₄ compound (in the middle of the range of compositions leading to pure spinel phase) will be used for the electrophoretic ink preparation.

Ni_{0.84}Al_{2.11}O₄ pigment characteristics

Prior to the synthesis of hybrid particles, measurement of the isoelectric point of the pigment needs to be carried out in order to get specific information about its charge. The pigments were dispersed in aqueous media at different pH between 2 to 12 and the electrophoretic mobility was measured for each sample. The isoelectric point (*i.e.* the point of zero charge) for this particular pigment was determined at 3.5 as shown in **Figure SI-2**. In a second step, the density and reflective point of the pigment were also calculated since it is important to have a pigment with a density close to that of the dispersant medium (Isopar-G with $\rho = 0.748$) as well as a high refractive index to improve the contrast ratio. The density ρ calculated using **Equation 1** is 4.2975 for a spinel structure Ni_{0.84}Al_{2.11}O₄. For a unit cell of Z monomeric units, the density ρ of the crystalline region is given by the equation 1, where Na is Avogadro's number (6.022×10^{23}), V is the volume of the unit cell and M_w is the molecular weight of the monomeric unit.

$$\rho = \frac{Z \cdot M_w}{Na \cdot V} \quad \text{Equation 1}$$

The Gladstone-Dale formula (**Equation 2**) has been used to estimate the refractive index of this powder. For that, ρ is the density of the complex oxide and the terms ρ_i and k_i are the mass fraction

and the molar refractivity in cm³/g of each oxide, respectively ($k_{NiO} = 0.2011$ and $k_{Al_2O_3} = 0.19125$ ³⁷). The refractive index is about 1.8316.

$$n = 1 + \rho(Ni_{0.84}Al_{2.11}O_4) \times \sum \rho_i \cdot k_i \quad \text{Equation 2}$$

Finally, the tinting strength has been measured in order to evaluate the contrast when this pigment is mixed with white one. Mixtures of the pigment with three different white powders (TiO₂ named γ , Al₂O₃ named β and CaCO₃ named α) which have different refractive index ($n(TiO_2) = 2.61$, $n(Al_2O_3) = 1.77$) and $n(CaCO_3) = 1.63$) were prepared. **Figure 5** shows the diffuse reflectance spectra of Ni_{0.84}Al_{2.11}O₄ pigment mixed with 50 wt.% of those white powders and then the evolution of the optical contrast for which white pigments have been taken as reference. Reflectance curves show an intermediate behaviour for mixtures in comparison with Ni_{0.84}Al_{2.11}O₄ and white pigments curves. The more the white pigment refractive index, the less the optical contrast. An optical contrast about 50-60% is obtained using calcium carbonate meanwhile with titanium oxide it is about 30-40%. Hence, the tinting strength of our cyan pigment is more or less equivalent as that of calcium carbonate.

Surface modification of the Ni_{0.84}Al_{2.11}O₄ compound

The modification of the inorganic pigments surface was performed to favor their dispersion in non-polar organic media (Isopar G). This preliminary modification is mandatory in order to synthesize hybrid polymer-inorganic particles by dispersion polymerization in Isopar G. The general procedure is schematized in **Figure 6**. Trimethoxysilane modifiers with different alkyl chains were grafted to the particle surface in order to increase the pigment hydrophobicity. The grafting is achieved via sol-gel chemistry during 20 h in dry toluene at 120°C (**Figure 6**) and leads to the dispersion of the pigments in non-polar media. Three parameters were studied; (i) the alkyl chain length (with n-Octyltrimethoxysilane OTS or n-Dodecyltrimethoxysilane DTS), (ii) the volume of modifier (10 or 5 v/v%) and (iii) a prior hydrolysis to increase the percentage of hydroxyl groups at the pigment surface. All these modifications are reported in **Table 5**.

These pigments have been characterized by (i) TGA to obtain the grafting percentage, (ii) DLS to determine the diameter of the hybrid particle, (iii) and Zetametry to evaluate the electrophoretic mobility (**Table 2**). According to the Table 2, the charge q , which is negative, do not depend on the alkyl chain length of the modifier. A prior hydrolysis does not increase the polymer content, so it is a step which is not necessary. One can observe, that lower the hybrid density, higher the alkyl chain, but it is not dependent on the modifier volume. The modification with DTS will be preferred at this step if we consider that the elaboration of a highly charged pigments with a low

density is predominant for this modification. **Figure SI-3** shows pigment without any modification dispersed in apolar media and pigments after silanization. The sedimentation of the pigment is slower after silanization compared to the dispersion of the pigment alone. Because of the low organic content, the density remains high, so the dispersion is still not very stable. It is surprising that the organic content is so low because the pigment exhibits an excess of Al-O(OH) bonds. It could be explained by a small specific surface of the pigment, in regards of the particle shape and its volume/surface ratio. In the following part, polymerization with MMA will be performed on each sample.

Hybrid particles synthesis in isopar G with MMA as a monomer

In order to decrease the density of the inorganic pigments and improve the colloidal stability in organic media, modified inorganic pigments were encapsulated into a polymer shell. As described in the literature,³⁸ Nitroxide-Mediated Radical Polymerization (NMRP) of methyl methacrylate (MMA) directly in a non-polar medium, using a poly(lauryl methacrylate) macro-initiator, led to core/shell hybrid particles (the general procedure is schematically represented in **Figure 7**). Lipophilic macroinitiators, covalently linked to the polymer shell, play the role of steric stabilizers thanks to their compatibility with the dispersing medium (isopar G).

For the dispersion polymerization, the molar mass of the poly(lauryl methacrylate) macro-initiator was fixed at 4500 g.mol⁻¹. We tried to keep the ratio between monomer and macro-initiator around 370, but depending on experimental conditions, it slightly varies between 340 and 400. (between Different modified pigments were used for the dispersion polymerization: with or without hydrolysis, OTS or DTS as modifying agent with two different feeding quantities (10 or 5 v/v%). Several dispersions in isopar G of hybrid particles have been obtained; **Table 3** summarizes the experimental conditions for all of them.

TEM imaging was performed on Ni_{0.84}Al_{2.11}O₄ modified with different alkyl chains size and modifier volume (**Figure 8**). One can observe a polymer shell around few aggregated pigments (in black) which allows a satisfying dispersion of the pigment particles. These observations were also confirmed by STEM imaging in dark-field mode (**Figure SI-4**). The electrophoretic mobility and the hydrodynamic radius of particles were determined by Phase Analysis Light Scattering (PALS) and Dynamic Light Scattering (DLS). All the hybrid particles characterizations are summarized in **Table 4**.

First, we can observe that pigments are positively charged after dispersion polymerization whereas they were negatively charged just after silanization. This can be explained by the use of MMA as

monomer. It was observed that the use of 4-Vinyl Pyridine (4-VP) in non-polar media, leading to positively charged particles even without charge control agent⁸. PMMA could behave in the same way, in that case. The mechanism is not well understood, but it can be explained by auto-ionization of solvent or impurities and/or adsorption of ionic species at the surface of PMMA³⁹. Polymer content, which is expressed in wt. % and determined by TGA is higher with OTS (smaller alkyl chains) than with the use of DTS (**Figure SI-5**). Particles average diameter has been determined by DLS. The particle size is two or three times higher after these two steps of surface modification in comparison with the pristine pigment. Those results are also confirmed by TEM pictures where pigments are aggregated inside a polymer shell. The use of DTS leads to low polymer contents. Indeed, as PMMA is a polar polymer, its precipitation around a very hydrophobic particle is more difficult. This could explain why modifications with OTS (which is less hydrophobic than DTS) allow to obtain a better polymer encapsulation. Furthermore, for both OTS and DTS, when a higher amount of silanization agent is used, we obtain low polymer contents and bigger particles. This is characteristic of an increase of inorganic pigment aggregation due to a too hydrophobic interface avoiding the precipitation of PMMA around the pigment. Consequently, the density, determined from the **Equation 3**, is lower when a low amount of OTS is used for silanization. The goal is to obtain a density close to the one of the dispersive medium (Isopar G, $d=0.749$) to obtain stable particles. A large amount of OTS would be preferred to obtain a higher charged particle (less polymer, more aggregated pigments), but a smaller amount of OTS is preferable to obtain a more stable ink thanks to small density particles.

Finally, we compared hybrid particles obtained with or without a prior hydrolysis. One can see it permits to improve a bit the grafting rate and the hybrid density but it increases the particles diameter and decreases the electrophoretic mobility and the charge. Therefore, this prior step does not allow any improvement of the ink qualities. In summary, a balance between all these parameters characterizations is needed to obtain a stable charged dispersion.

The analysis of the ink stability was performed with Turbiscan® Lab Stability Analyzer. By this way, it is possible to determine an index of sedimentation (TSI) which is specific to the apparatus and which is obtained from **Equation 5** (see experimental part). The lower the sedimentation index, the higher stability inks. All results are gathered in **Figure 10** and **Table 4**. Photography of the most stable, an intermediate and the least stable dispersions are presented in **Figure 9**. As expected, the more stable ink from $\text{Ni}_{0.84}\text{Al}_{2.11}\text{O}_4$ pigments is obtained when a low quantity of OTS (5 v/v%) is used as modification agent before the polymerization. This is in correlation with the hybrid particles characterization (**Table 4**). Indeed, the most stable particles are the ones

with the highest polymer content, the lowest density and the smallest diameter (limiting aggregation). It is interesting to notice that prior pigment hydrolysis does not improve (or degrade) significantly the ink stability. Nevertheless, despite there is partial decantation after 24 hours in the two worst cases, it is important to note that for application a stability of few hours, even few minutes could be enough. Indeed, in an EPID, it is possible to apply regularly an electric field for few milliseconds in order to maintain the image.

Finally, we tried to estimate the capability of re-dispersion after decantation. **Figure SI-6** shows the TSI curves obtained immediately after polymerization and after remixing of aged dispersions. In both cases, similar behaviors were observed highlighting the possibility to remix dispersions after sedimentation.

3. CONCLUSION

Cyan NiAl_2O_4 spinel pigments have been synthesized by a sol-gel route. The preparation of aluminum over-stoichiometric pigments results in a single phase. The cation distribution of $\text{Ni}_{0.84}\text{Al}_{2.11}\square_{0.05}\text{O}_4$ compound inside the spinel crystalline framework has been extracted from Rietveld refinements using different choices for vacancy location. The refinement quality is only weakly impacted by the vacancy location model. However, as the cationic distribution is significantly impacted by the vacancy location, it is difficult to determine an accurate cation distribution, even if the occurrence of cationic vacancies in octahedral site leads to the lowest reliability factor R_B . Nonetheless, in all cases, a distribution of nickel (II) chromophores in both tetrahedral and octahedral sites is obtained. Considering the structural hypothesis where cationic vacancies are located in Oh site, the proportion of Ni^{2+} in Td and Oh sites for the $\text{Ni}_{0.84}\text{Al}_{2.11}\square_{0.05}\text{O}_4$ composition should be after refinement 46% (Td) : 54% (Oh), close to fifty-fifty corresponding to a partially inverted spinel. This is confirmed from the absorption bands indexed on optical spectra where d-d transitions related to Td (high intensity of the triplet around 650 nm due to the acentric character of Td site) and Oh environments (the lowest intensity bands around 700 nm related to the centrosymmetric Oh site) are clearly visible. This study showed hence the difficulty to control the cyan coloration of such compounds. On the basis of optical spectra, in the series of pure phases with Ni/Al = 0.35, 0.40, 0.45 atomic ratios, the higher the Al content for Ni/Al=0.45 value, the lower the Ni^{2+} rate in Td site. Whatever Ni/Al molar ratio ranging from 0.3 to 0.4, experimental colorimetric parameter $L^*a^*b^*$ are very closed to the theoretical ones for the cyan color and this can be related to a higher amount of Ni^{2+} in Td environment.

Colored and charged electrophoretic inks were successfully synthesized via the encapsulation of the as-prepared inorganic pigments directly in a non-polar medium. NMRP of MMA in the presence of pigments and a hydrophobic macro-initiator leads to the formation of core-shell hybrid particles. The particle charge is dependent on the nature of the pigment surface, *i.e.* the IEP of the pigment, the type of monomer used and the polymer grafting rate. The use of MMA as monomer induced a change of the hybrid charge from negative to positive. These inks were further formulated without the use of any additive and the study of their stability has shown that the use of OTS as surface modifier OTS inks are adequate for EPID applications.

Further works will consist in mixing those pigments with white negatively charged hybrid particles to produce a dual-colored electrophoretic ink for the next generation of colored EPID.

4. EXPERIMENTAL PART

Pigment synthesis

NiAl₂O₄ pigments were synthesized by a sol gel process: the Pechini route. This process is based on cations chelation by citric acid (CA), (Aldrich, ACS reagent > 99.5%) and on polyesterification between CA and ethylene glycol (EG), (Alfa Aesar, purity over 99%) leading to the formation of a polycationic resin. Aqueous solutions of citrate were prepared by dissolving CA and EG in a minimal volume of water. Then, cationic salts: NiCl₂·6H₂O (Alfa Aesar, purity over 98%) and AlCl₃·6H₂O (Sigma Aldrich, purity 99%) were added in stoichiometric proportion to the acid solution. CA and EG are in equimolar proportion and the CA/cations molar ratio equals 4:1. EG-CA polymerization was promoted by removing water with continuous heating on a hot plate. The as-prepared highly viscous mixtures were thermally treated in two steps: a first calcination at 400°C under air to remove organics components, then, an annealing step for 10 hours at 1400°C.

Pigment functionalization

As a representative experiment, a 100 ml two necked flask was used and 326 mg of inorganic pigments were dispersed in 10 mL of dried toluene. The mixture was sonicated for 30 minutes in an ultrasonic bath and heated at 120°C for 18 hours under magnetic stirring; 10 or 5 v/v% of OTS n-octyltrimethoxysilane, (OTS), (ABCR, 97%) or n-dodecyltrimethoxysilane (DTS), (TCI, 93%) was added to the mixture. The dispersion reaction was washed by centrifugation/redispersion cycles in dried toluene. The modified pigments were then dried at 65°C for one-night long. **Table 5** summarizes the experimental conditions used for these pigment modifications. Optionally, a preliminary hydrolysis step was performed to observe an eventual impact of surface hydroxyl groups on the pigment modification process. For this, in a 100 mL two necked flask 1 g of pigment

are dispersed into 5 g of hydrogen peroxide (30%). The mixture was sonicated during 30 minutes and heated at 105°C during 4 hours. The dispersion reaction was washed by centrifugation/redispersion cycles in deionized water. The resulting powder was dried for few hours in a vacuum oven.

Hybrid particles synthesis

For a typical Nitroxide Mediated Radical Polymerization (NMRP) via dispersion in Isopar G (commercial isoparaffinic hydrocarbon, Exxon Mobil Chemical), 5.0×10^{-4} mol of lauryl acrylate-SG1 macroinitiator⁴⁰ and 200 mg of the modified pigments were firstly dispersed in 10 mL Isoparaffin G. This solution was ultra-sonicated during 1 hour. Then the solution was outgassed by bubbling argon for 1 additional hour; this step including the addition of Methyl methacrylate (MMA), (Acros 99%) after 30 minutes of nitrogen bubbling. Finally, the mixture was heated at 120°C under mechanical stirring for 19 hours. Finally, the as-prepared particle suspension (*i.e.* as-prepared electrophoretic ink) was cooled down and purified by 3 cycles of centrifugation and redispersion in Isoparaffin G to remove the residual monomers.

Characterization techniques

X-Ray diffraction (XRD) measurements were carried out on a PANalytical X'PERT PRO diffractometer equipped with an X-celerator detector, using $\text{Cu}(\text{K}\alpha_1/\text{K}\alpha_2)$ radiation. The spectra were recorded on 5-120° 2θ range with a time per step chosen in order to get at least 10,000 cps in intensity for the main diffractogram peak. Diffractograms were refined with the Rietveld refinement method using FULLPROF® program package. The unit-cell parameters, the atomic positions, the cationic distribution (cation inversion parameter) were then refined (with fixed Debye Waller factors) on the basis of the $Fd-3m$ space group corresponding to the spinel structure. The peak profiles are fitted with the Caglioti function, *i.e.* considering isotropic crystallites. Uncertainties can be calculated from the standard deviation proposed by the software; these uncertainties being approximated in all cases to the decade higher, all reported results are limited to their last significant digit.

UV-Vis-NIR diffuse reflectivity ($R(\lambda)\%$) spectra – herein, presented after Kubelka-Munk transformation: $\text{KM}(\lambda) = (1 - R(\lambda)\%)^2 / (2R(\lambda)\%)$, - were recorded at room temperature from 200 to 2500 nm with a step of 1 nm and a band length of 2 nm on a Cary 17 spectrophotometer using an integration sphere. Halon polymer was used as white reference for the blank. A mathematic treatment of the obtained spectra allowed the determination of the $L^*a^*b^*$ space colorimetric parameters. The first step of the treatment consists in obtaining the XYZ tri-stimulus values

(defined by the CIE, 1964) from the integration (on the visible range, *i.e.* from $\lambda = 380$ nm up to 780 nm) of the product of $x(\lambda)$, $y(\lambda)$ or $z(\lambda)$ functions (CIE – 1964) with the diffuse reflectance spectra function: $X = \int x(\lambda) \cdot R(\lambda) d\lambda$. Then, the transfer equations defined by the CIE, 1976, from XYZ space to the $L^*a^*b^*$ space, were used in order to obtain the $L^*a^*b^*$ chromatic parameters.

The morphology of $Ni_{1-x}Al_{2+2x/3}O_4$ nanoparticles was evaluated by transmission electronic microscopy (TEM). These characterizations were performed on TEM Jeol 2100F operated at 200 kV with a LaB_6 gun. The theoretical resolution (FWHM) was nominally 2.3 Å. The quantification of Ni and Al concentration were performed by Energy Dispersive X-Ray Spectrometry (EDX) considering K lines intensities and integration. Samples were prepared by dissolving a few milligrams of powder in ethanol directly depositing one drop of the as-prepared suspension on a copper grid.

Hybrid particles were first imaged by transmission electron microscopy (TEM) using a JEOL 1400+ at 120kV equipped with a LaB_6 filament and a GATAN camera with condenser diaphragm. STEM observations were carried out on a JEOL 7800 using an acceleration voltage of 15 kV and the transmission electron detector (TED) in dark-field mode.

Thermogravimetric analyses (TGA) from 20°C to 700°C at 10°C.min⁻¹ were performed under nitrogen environment with a Q500 apparatus from TA Instrument.

The density of the as-prepared hybrid particles was estimated according to the pigment density (ρ_{pig}) and the polymer density (ρ_{pol}) reported from the literature using the weight fractions of the pigment, wc_{pig} , and the polymer, wc_{pol} , deduced from the thermal gravimetric analysis (see Equation 3) [5].

$$\rho = \frac{1}{\frac{wc_{pig}}{\rho_{pig}} + \frac{wc_{pol}}{\rho_{pol}}} \quad \text{Equation 3}$$

The electrophoretic mobility and the hydrodynamic radius of colloids were determined by Phase Analysis Light Scattering (PALS) and Dynamic Light Scattering (DLS), respectively, on a Nano ZS Malvern Instrument using a wavelength of $\lambda = 633$ nm at a fixed angle $\theta=90^\circ$. A square shaped wave electric field from 2.5 to 20 kV.m⁻¹ was applied using a dip cell designed for measurement in a non-aqueous environment. Each sample was measured 3 times (15 runs/measurement).

The q global charge of hybrid particles was determined using the equation reported by Fang and *al.*[6] (see Equation 4, with v : the electrophoretic speed (m.s⁻¹), E : the applied electrophoretic

potential (V), R: the average radius of the particles; g: 9.8m.s⁻²; η: the viscosity of the electrophoretic medium in mPa.s).

$$v = \frac{(qE + \frac{4}{3}\pi R^3 g(\rho_{pi}g - \rho_{pol}))}{6\pi R\eta} \quad \text{Equation 4}$$

Stability of the inks was estimated using a Turbiscan® lab stability analyzer in order to follow the stability of the colloidal dispersions over time using the transmittance and backscattering ratio of a pulsed near infrared light (λ = 880 nm). The transmittance detector received the light which passed through the dispersion at an angle of 180° with the respect to the source, while the backscattering detector received the light scattered backward by the dispersion at an angle of 45°. The analysis of the stability was carried out as a variation of backscattering (BS) and transmittance (T%) profiles. Equation 5 is used for the calculation of the Turbiscan Stability Index (TSI). TSI is obtained by analyzing the evolution versus time of evolution of the transmission of each suspension layer (at different height: h), and normalizing the result by the total analyzed thickness (H) in order to obtain a result which is independent of the quantity of sample in the measuring tube.

$$TSI(\text{turbiscan stability index}) \quad \text{Equation 5}$$

$$= \sum_i \frac{\sum_h |T\%_t(h) - T\%_{t-1}(h)|}{H}$$

Where h and H is the selected height and the total height of sample respectively.

FIGURES

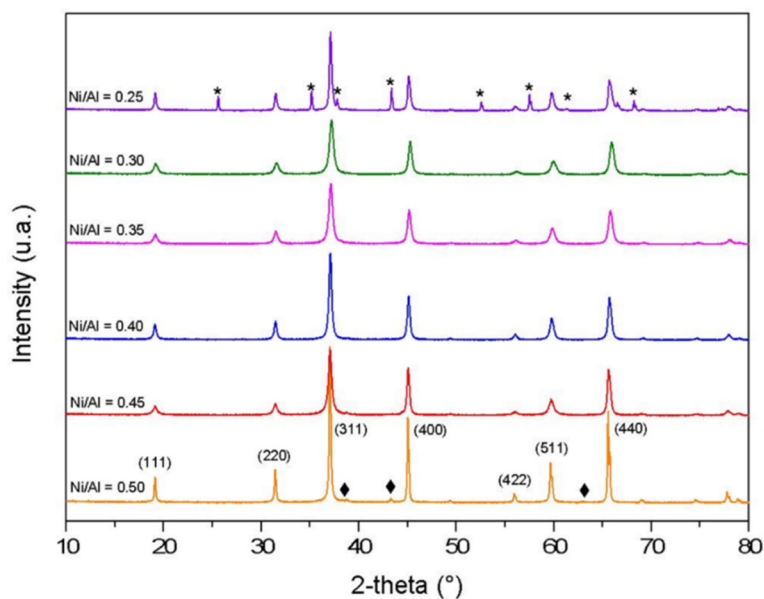


Figure 1. XRD patterns of $\text{NiAl}_{2+x}\text{O}_{4+\square}$ compounds (with Ni/Al = 0.5, 0.45, 0.4, 0.35, 0.3 or 0.25) prepared from Pechini route followed by post-annealing at 1400°C. Al_2O_3 (*) and NiO (◆) impurities are shown.

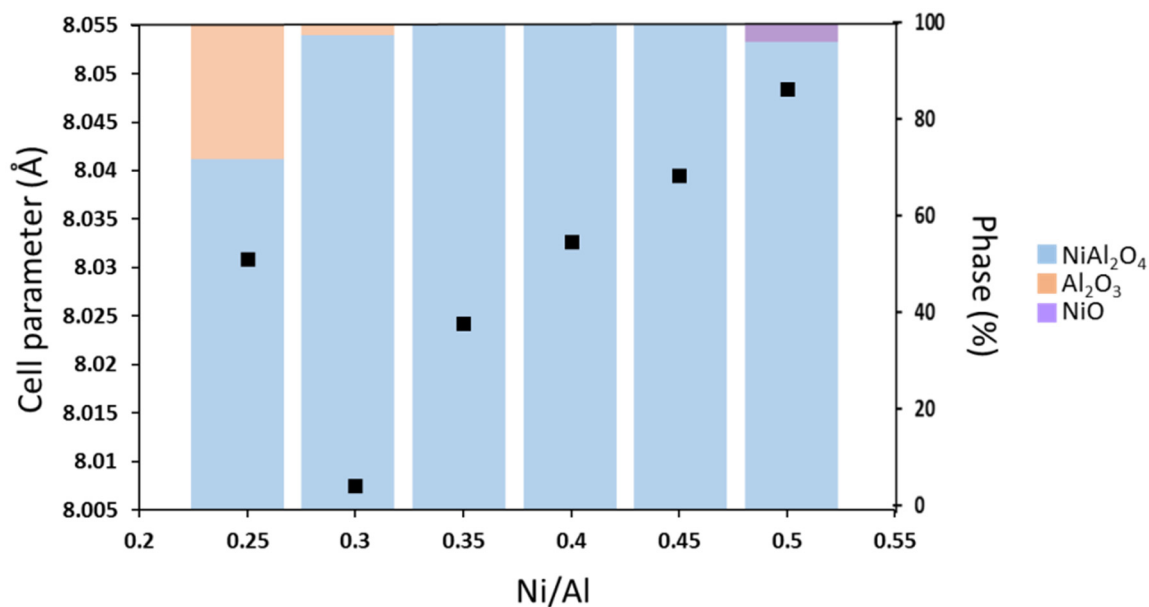


Figure 2. Evolution of the cell parameter of the main spinel phase in the $\text{Ni}_{1-x}\text{Al}_{2+2x/3}\text{O}_4$ compounds; weight percentage of each phases (NiAl_2O_4 , NiO and Al_2O_3) within the $\text{NiAl}_{2+x}\text{O}_{4+\square}$ compounds.

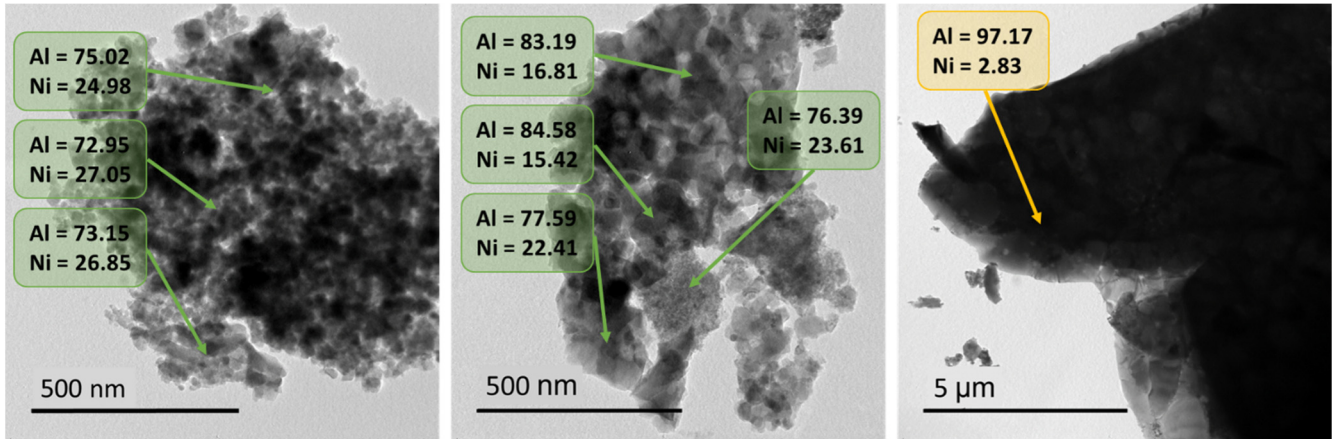


Figure 3. TEM micrographs of $\text{Ni}_{1-x}\text{Al}_{2+2x/3}\text{O}_4$ samples with Ni/Al theoretical ratio equal to 0.40 (left side) and 0.25 (central to right side with different zone area and magnificence).

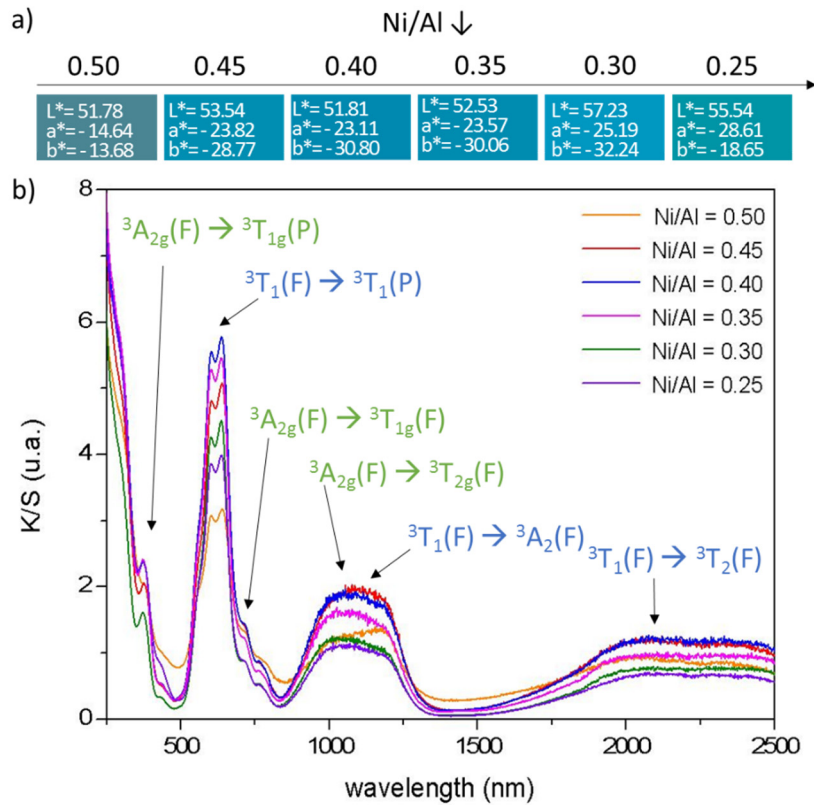


Figure 4. a) $L^*a^*b^*$ colour parameters and b) K/S spectra of $\text{Ni}_{1-x}\text{Al}_{2+2x/3}\text{O}_4$ compounds (with Ni/Al = 0.5, 0.45, 0.4, 0.35, 0.3 or 0.25). Transitions corresponding to nickel (II) in octahedral (blue) and tetrahedral (green) coordination are identified.

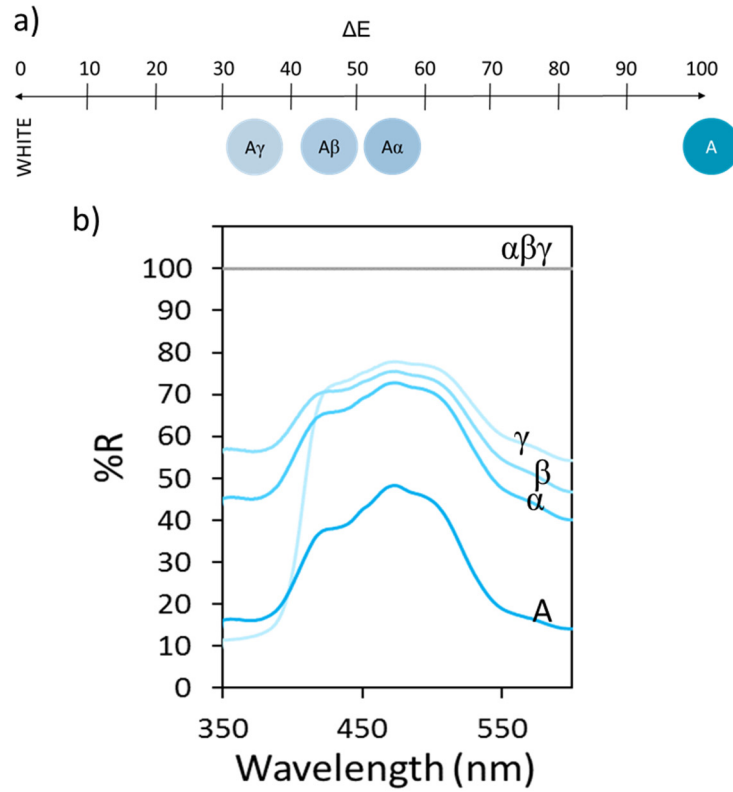


Figure 5. a) Evolution of the optical contrast and b) Diffuse reflectance spectra of $Ni_{1-x}Al_{2+2x/3}O_4$ (A) pigment and of mixtures with 50 wt.% of $CaCO_3$ (α), Al_2O_3 (β) and TiO_2 (γ).

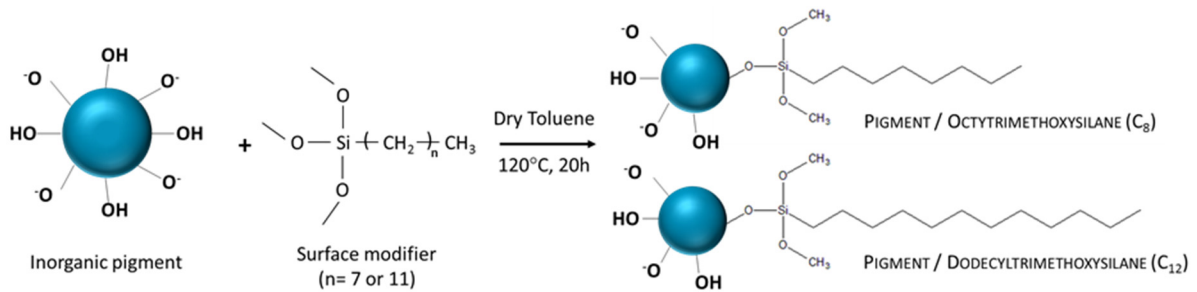


Figure 6. Surface modification of inorganic pigments.

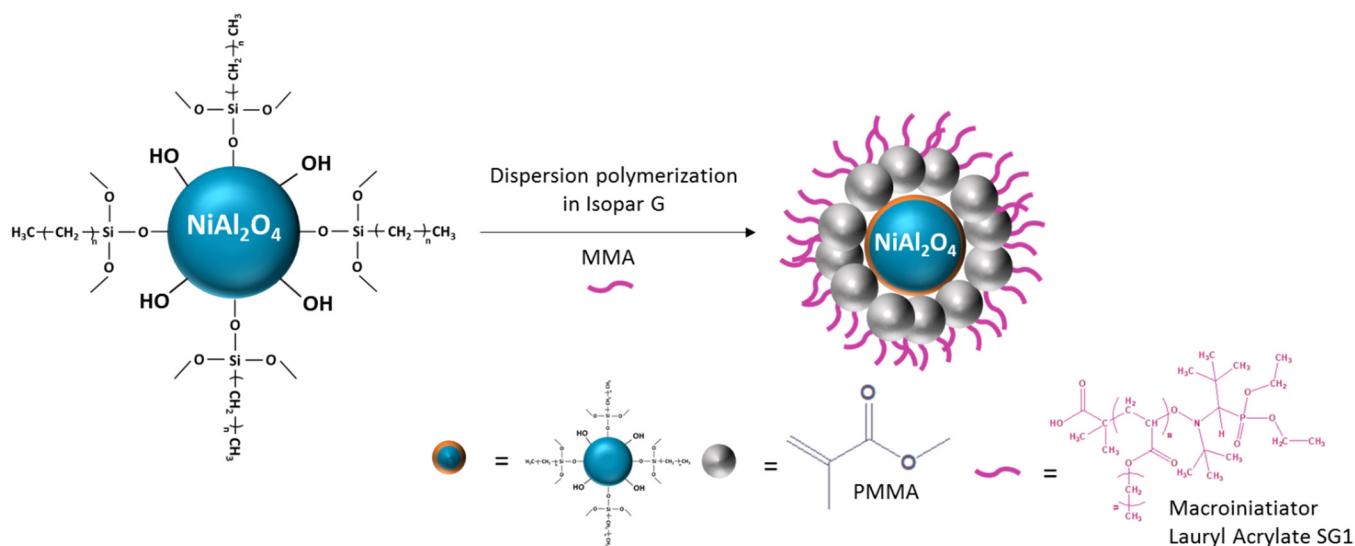
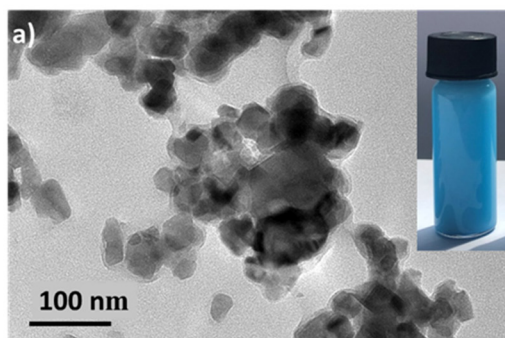
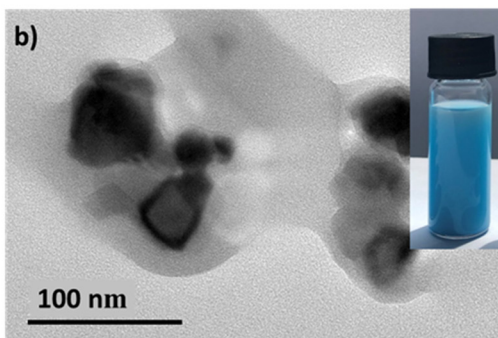


Figure 7. Hybrid particles synthesis via NMRP in isopar G as a solvent

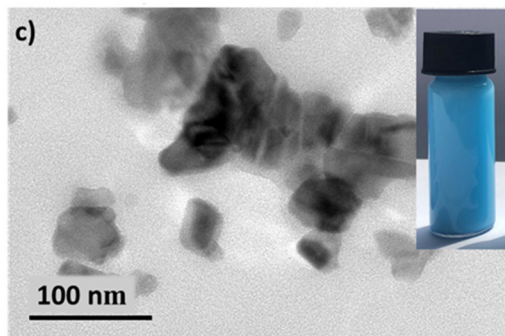
10% OTS (Hyd) - MMA



10% OTS - MMA



5% OTS (Hyd) - MMA



5% OTS - MMA

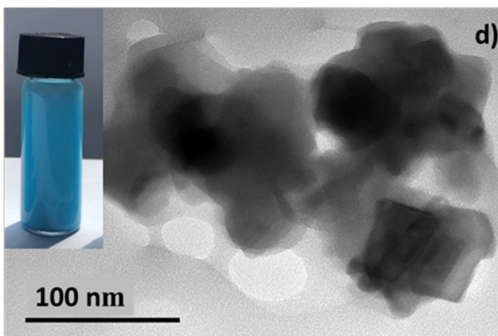


Figure 8. TEM micrographs of $\text{Ni}_{0.84}\text{Al}_{2.11}\square_{0.05}\text{O}_4$ hybrid. a) Hydrolysed, modified with 10 v/v% of OTS and polymerised with 10 v/v% of MMA, b) Modified with 10 v/v% of OTS and polymerised with 10 v/v% of MMA c) Hydrolysed, modified with 5 v/v% of OTS and polymerised with 10 v/v% of MMA d) Modified with 5 v/v% of OTS and polymerised with 10 v/v% of MMA

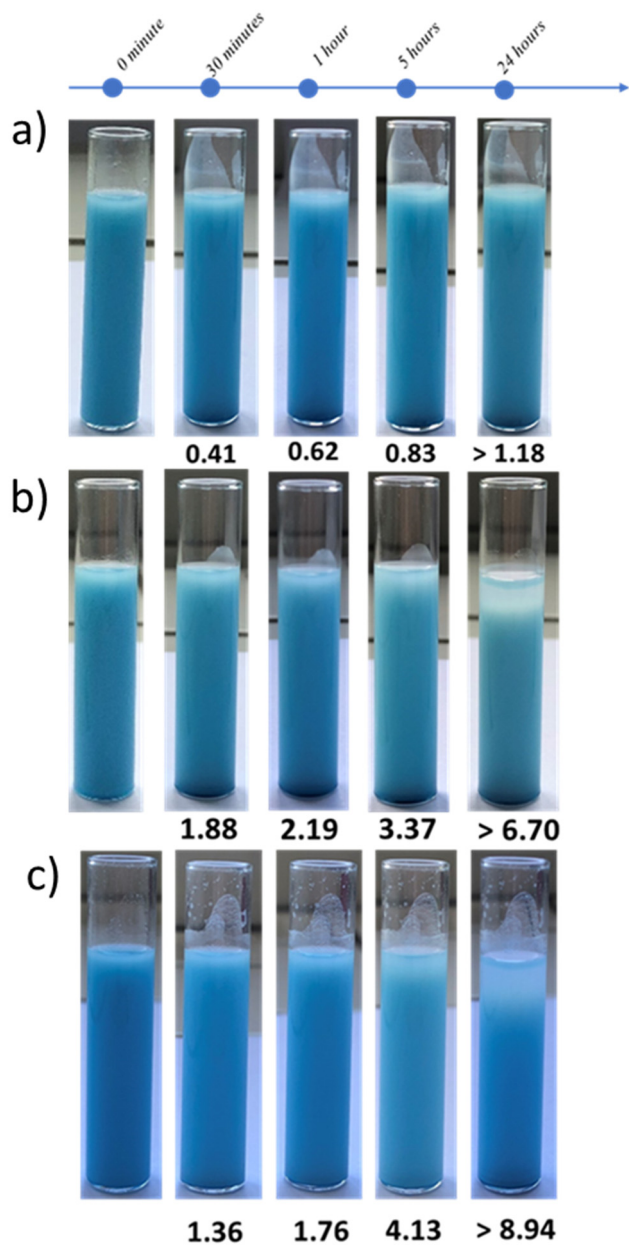


Figure 9. Pictures of samples as function of time of three dispersions of hybrid particles polymerised with 10 v/v% of MMA and dispersed in Isopar-G, a) Modified with 5 v/v% of OTS, b) Modified with 10 v/v% of OTS and c) Modified with 10v/v% of DTS. TSI are indexed in each picture.

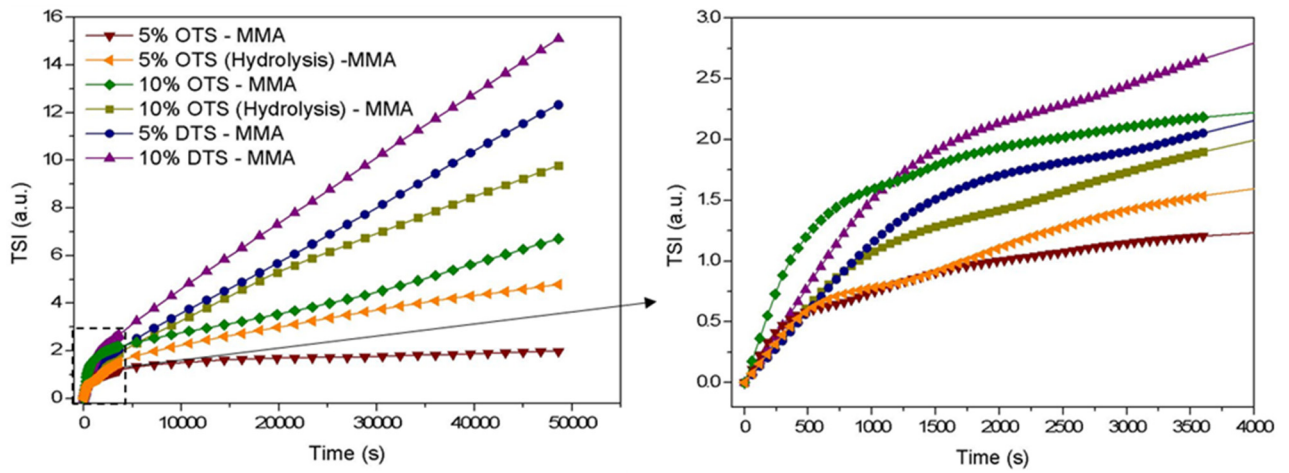


Figure 10. Evolution of the Time Sedimentation Index (TSI) with the time for hybrid particles dispersed in isopar-G during 13 hours. On the right, a zoom of those curves has been made.

TABLES

Table 1. Occupancy rate and correlation factors issued from three kinds of Rietveld refinement.
(If there is no vacancy, if the vacancy is in an octahedral or in a tetrahedral site).

Atom	Occupancy rate / NiAl ₂ O ₄	Occupancy rate / vacancy [6]	Occupancy rate / vacancy [4]
Ni [4]	0.007	0.016	0.023
Ni [6]	0.034	0.019	0.012
Al [4]	0.034	0.025	0.016
Al [6]	0.049	0.062	0.072
R _B	2.78	1.89	2.12
R _p	10.9	10.4	10.6
Composition	(Ni _{0.18} Al _{0.82})[Ni _{0.82} Al _{1.18}]O ₄	(Ni _{0.39} Al _{0.61})[Ni _{0.45} Al _{1.50} □ _{0.05}]O ₄	(Ni _{0.56} Al _{0.39} □ _{0.05})[Ni _{0.29} Al _{1.71}]O ₄

Table 2. Characterization of the modified inorganic pigments: organic content, diameter, electrophoretic mobility, density and charge in Isopar G

Pigment	Organic content (%wt)	Hybrid density (u.a.)	Particle diameter (nm)	Electrophoretic mobility (10 ⁴ μm ² /Vs)	Charge (eV)
NiAl ₂ O ₄ -5%OTS	2.25	4.11	187	-0.3692	-1 464
NiAl ₂ O ₄ -Hyd-5%OTS	2.25	4.11	298	-0.0851	-473
NiAl ₂ O ₄ -10%OTS	2.5	4.07	280	-0.3150	-1 835
NiAl ₂ O ₄ -Hyd-10%OTS	1	4.32	212	-0.1719	-755
NiAl ₂ O ₄ -5%DTS	2.75	4.04	251	-0.2908	-1 525
NiAl ₂ O ₄ -10%DTS	2.75	4.04	202	-0.2672	-1 137

Table 3. Experimental conditions of hybrid particles syntheses *via* NMRP polymerization with MMA as monomer and polylaurylacrylate as macroinitiator ($M_n = 4500$ g/mol) in isopar G, on previously modified pigments.

Hybrid Particle	[pigment] g.L ⁻¹	[Ma(LA)] (mmol.L ⁻¹)	[MMA] (mol.L ⁻¹)	$\frac{[monomer]}{[macroinitiator]}$
NiAl ₂ O ₄ -5%OTS-MMA	19.91	2.72	0.94	334
NiAl ₂ O ₄ -Hyd-5%OTS-MMA	19.96	2.41	0.94	378
NiAl ₂ O ₄ -10%OTS-MMA	20.31	2.53	0.94	360
NiAl ₂ O ₄ -Hyd-10%OTS-MMA	19.96	2.24	0.94	406
NiAl ₂ O ₄ -5%DTS-MMA	20.45	2.40	0.94	379
NiAl ₂ O ₄ -10%DTS-MMA	21.30	2.60	0.94	350

Table 4. Characterization of hybrid particles obtained via NMR polymerization with MMA on inorganic pigments.

Hybrid Particle	Polymer content (%wt)	Hybrid density (u.a.)	Particle diameter (nm)	Electrophoretic mobility (10 ⁴ μm ² /Vs)	Charge (eV)	TSI	
						1h	12h
NiAl ₂ O ₄ -5%OTS-MMA	61	1.36	652	+0.072	+1 143	1	2
NiAl ₂ O ₄ -Hyd-5%OTS-MMA	62	1.34	597	+0.062	+895	2	5
NiAl ₂ O ₄ -10%OTS-MMA	37	1.87	701	+0.094	+1 724	2	7
NiAl ₂ O ₄ -Hyd-10%OTS-MMA	45	1.66	1 070	+0.066	+2 411	2	10
NiAl ₂ O ₄ -5%DTS-MMA	18.3	2.66	466	+0.052	+675	2	12
NiAl ₂ O ₄ -10%DTS-MMA	27.5	2.20	732	+0.025	+849	3	15

Table 5. Experimental conditions for pigment modification.

Pigment	Hydrolysis	Modifier	[pigment] g.L⁻¹	V_{modifiant} v/v%
NiAl ₂ O ₄ -5%OTS	No	OTS	32.73	5
NiAl ₂ O ₄ -Hyd-5%OTS	Yes	OTS	32.61	5
NiAl ₂ O ₄ -10%OTS	No	OTS	32.68	10
NiAl ₂ O ₄ -Hyd-10%OTS	Yes	OTS	32.56	10
NiAl ₂ O ₄ -5%DTS	No	DTS	32.56	5
NiAl ₂ O ₄ -10%DTS	No	DTS	32.67	10

ASSOCIATED CONTENT

Supporting Information.

Rietveld refinement, isoelectric point determination, STEM blackfield images, TGA curves and evolution of the time sedimentation index of the inks.

The Supporting Information is available free of charge on the ACS Publications website at <http://pubs.acs.org>.

AUTHOR INFORMATION

Corresponding Author

* Corresponding authors : cyril.brochon@enscbp.fr and manuel.gaudon@icmcb.cnrs.fr

Author Contributions

The manuscript was written through contributions of all authors.

ACKNOWLEDGMENT

Authors want to thank Equipex ELORPrintTec facilities (ANR-10-EQPX-28-01)

REFERENCES

- [1] Comiskey, B.; Albert, J.; Yoshizawa, H.; Jacobson, J. An electrophoretic ink for all-printed reflective electronic displays. *Nature*. **1998**, *394*, 6690, 253–255.
- [2] Rogers, J. A.; Bao, Z. Printed plastic electronics and paperlike displays. *J. Polym. Sci. Part Polym. Chem.* **2002**, *40*, 20, 3327–3334.
- [3] Kim, C. A.; Joung, M. J.; Ahn, S. D.; Kim, G. H.; Kang, S.-Y.; You, I.-K.; Oh, J.; Myoung, H. J.; Baek, K. H.; Suh, K. S.; Microcapsules as an electronic ink to fabricate color electrophoretic displays. *Synth. Met.* **2005**, *151*, 3, 181–185.
- [4] Badila, M.; Hébraud, A.; Brochon, C.; Hadziioannou, G. Design of Colored Multilayered Electrophoretic Particles for Electronic Inks. *ACS Appl. Mater. Interfaces*. **2011**, *3*, 9, 3602–3610.
- [5] Yu, D.-G.; An, J. H. Preparation and characterization of titanium dioxide core/polymer shell hybrid composite particles prepared by emulsion polymerization. *J. Appl. Polym. Sci.* **2004**, *92*, 5, 2970–2975.
- [6] Fang, Y.; Wang, J.; Li, L.; Liu, Z.; Jin, P.; Tang, C. Preparation of chromatic composite hollow nanoparticles containing mixed metal oxides for full-color electrophoretic displays. *J. Mater. Chem. C*. **2016**, *4*, 24, 5664–5670.
- [7] Peng, B.; Li, Y.; Li, J.; Lu, H.; Xie, J.; Ren, X.; Cao, Y.; Wang, N.; Meng, X.; Deng, L.; Guo, Z. Monodisperse light color nanoparticle ink toward chromatic electrophoretic displays. *Nanoscale*. **2016**, *8*, 21, 10917–10921.
- [8] Noël, A.; Mirbel, D.; Charbonnier, A.; Cloutet, E.; Hadziioannou, G.; Brochon, C. Synthesis of charged hybrid particles via dispersion polymerization in nonpolar media for color electrophoretic display application. *J. Polym. Sci. Part Polym. Chem.* **2017**, *55*, 2, 338–348.
- [9] Yu, D.-G.; An, J. H.; Bae, J.-Y.; Ahn, S. D.; Kang, S.-Y.; Suh, K.-S. Negatively Charged Ultrafine Black Particles of P(MMA- *c o* -EGDMA) by Dispersion Polymerization for Electrophoretic Displays. *Macromolecules*. **2005**, *38*, 17, 7485–7491.
- [10] Wen, T.; Meng, X.; Li, Z.; Ren, J.; Tang, F. Pigment-based tricolor ink particles via mini-emulsion polymerization for chromatic electrophoretic displays. *J. Mater. Chem.* **2010**, *20*, 37, 8112.
- [11] Werts, M. P. L.; Badila, M.; Brochon, C.; Hébraud, A.; Hadziioannou, G. Titanium Dioxide- Polymer Core–Shell Particles Dispersions as Electronic Inks for Electrophoretic Displays. *Chem. Mater.* **2008**, *20*, 4, 1292–1298.
- [12] Regan, M. T. Novel phthalocyanine pigments. **1983**.
- [13] El Jazouli, A.; Tbib, B.; Demourgues, A.; Gaudon, M. Structure and colour of diphosphate pigments with square pyramid environment around chromophore ions (Co^{2+} , Ni^{2+} , Cu^{2+}). *Dyes Pigments*. **2014**, *104*, 67–74.
- [14] Robertson, L.; Duttine, M.; Gaudon, M.; Demourgues, A. Cobalt–Zinc Molybdates as New Blue Pigments Involving Co^{2+} in Distorted Trigonal Bipyramids and Octahedra. *Chem. Mater.* **2011**, *23*, 9, 2419–2427.
- [15] Giannakas, A. E.; Ladavos, A. K.; Armatas, G. S.; Pomonis, P. J. Surface properties, textural features and catalytic performance for NO + CO abatement of spinels MAl_2O_4 (M = Mg, Co and Zn) developed by reverse and bicontinuous microemulsion method. *Appl. Surf. Sci.* **2007**, *253*, 16, 6969–6979.
- [16] Sickafus, K. E.; Wills, J. M.; Grimes, N. W. Structure of spinel. *J. Am. Ceram. Soc.* **1999**, *82*, 12, 3279–3292.
- [17] Areán, C. O.; Mentruit, M. P.; López, A. L.; Parra, J. B. High surface area nickel aluminate spinels prepared by a sol–gel method. *Colloids Surf. Physicochem. Eng. Asp.* **2001**, *180*, 3, 253–258.

- [18] Bayal, N.; Jeevanandam, P. Synthesis of CuO@NiO core-shell nanoparticles by homogeneous precipitation method. *J. Alloys Compd.* **2012**, *537*, 232–241.
- [19] Li, C. Y.; Zhang, H. J.; Chen, Z. Q. Reaction between NiO and Al₂O₃ in NiO/γ-Al₂O₃ catalysts probed by positronium atom. *Appl. Surf. Sci.* **2002**, *266*, 17–21.
- [20] Amini, M. M.; Torkian, L. Preparation of nickel aluminate spinel by microwave heating. *Mater. Lett.* **2002**, *57*, 3, 639–642.
- [21] Peelamedu, R. D.; Roy, R.; Agrawal, D. K. Microwave-induced reaction sintering of NiAl₂O₄. *Mater. Lett.* **2002**, *55*, 234–240.
- [22] Jeevanandam, P.; Kolytyn, Y.; Gedanken, A. Preparation of nanosized nickel aluminate spinel by a sonochemical method. *Mater. Sci. Eng. B.* **2002**, *90*, 125–132.
- [23] Gama, L.; Ribeiro, M. A.; Barros, B. S.; Kiminami, R. H. A.; Weber, I. T.; Costa, A. C. F. M. Synthesis and characterization of the NiAl₂O₄, CoAl₂O₄ and ZnAl₂O₄ spinels by the polymeric precursors method. *J. Alloys Compd.* **2009**, *483*, 1–2, 453–455.
- [24] Suciú, C.; Patron, L.; Mindru, I.; Carp, O. Nickel aluminate spinel by thermal decomposition of polynuclear malate complexes. *Rev. Roum. Chim.* **2006**, *51*, 5, 385.
- [25] Nazemi, M. K.; Sheibani, S.; Rashchi, F.; Gonzalez-DelaCruz, V. M.; Caballero, A. Preparation of nanostructured nickel aluminate spinel powder from spent NiO/Al₂O₃ catalyst by mechano-chemical synthesis. *Adv. Powder Technol.* **2012**, *23*, 6, 833–838.
- [26] Ribeiro, N. F. P.; Neto, R. C. R.; Moya, S. F.; Souza, M. M. V. M.; Schmal, M. Synthesis of NiAl₂O₄ with high surface area as precursor of Ni nanoparticles for hydrogen production. *Int. J. Hydrog. Energy.* **2010**, *35*, 21, 11725–11732.
- [27] Leal, E.; De Melo Costa, A. C. F.; De Freitas, N. L.; De Lucena Lira, H.; Kiminami, R. H. G. A.; Gama, L. NiAl₂O₄ catalysts prepared by combustion reaction using glycine as fuel. *Mater. Res. Bull.* **2011**, *46*, 9, 1409–1413.
- [28] Cooley, R. F.; Reed, J. S. Equilibrium cation distribution in NiAl₂O₄, CuAl₂O₄, and ZnAl₂O₄ spinels. *J. Am. Ceram. Soc.* **1972**, *55*, 8, 395–398.
- [29] Han, Y. S.; Li, J. B.; Ning, X. S.; Yang, X. Z.; Chi, B. Study on NiO excess in preparing NiAl₂O₄. *Mater. Sci. Eng. A.* **2004**, *369*, 1–2, 241–244.
- [30] Subramanian, R.; Higuchi, M.; Dieckman, R. Growth of nickel aluminate single crystals by the floating zone method. *J. Cryst. Growth.* **1994**, *143*, 3–4, 311–316.
- [31] Zhou, R.-S.; Snyder, R. L. Structures and transformation mechanisms of the η, γ and β transition aluminas. *Acta Crystallogr. B.* **1991**, *47*, 5, 617–630.
- [32] Smrcok, L.; Langer, V.; Krestan, J. γ-Alumina: a single-crystal X-ray diffraction study. *Acta Crystallogr. C.* **2006**, *62*, 9, 83–84.
- [33] Tanabe, Y.; Sugano, S. On the absorption spectra of complex ions I. *J. Phys. Soc. Jpn.* **1954**, *9*, 5, 753–766.
- [34] Tanabe, Y.; Sugano, S. On the absorption spectra of complex ions II. *J. Phys. Soc. Jpn.* **1954**, *9*, 5, 766–779.
- [35] Tanabe, Y.; Sugano, S. On the absorption spectra of complex ions III. *J. Phys. Soc. Jpn.* **1956**, *11*, 8, 864–877.
- [36] Tanabe, Y.; Kamimura, H. On the absorption spectra of complex ions IV. *J. Phys. Soc. Jpn.* **1958**, *13*, 4, 394–411.
- [37] Tilley, R. Colour and optical properties of materials, Wiley; **2000**.
- [38] Charbonnier, A.; Brochon, C.; Cloutet, E.; Navarro, C.; Hadziioannou, G. Synthesis of functional polymer particles by dispersion polymerization in organic media: A tool toward stable electrophoretic inks. *J. Polym. Sci. Part Polym. Chem.* **2013**, *51*, 21, 4608–4616.
- [39] Smith, G.N.; Hallett, J.E.; Easto, J. *Soft Matter.* **2015**, *11*, 8029–8041
- [40] Noel, A.; Mirbel, D.; Cloutet, E.; Fleury, G.; Schatz, C.; Navarro, C.; Hadziioannou, G.; Brochon, C. Tridodecylamine, an efficient charge control agent in non-polar media for electrophoretic inks application. *Appl. Surf. Sci.* **2018**, *428*, 870–876.

Table of Contents Only

